Journal of Materials Chemistry B

ROYAL SOCIETY OF CHEMISTRY

PAPER

View Article Online
View Journal | View Issue

Cite this: J. Mater. Chem. B, 2023, 11, 9950

Etamsylate loaded oxidized Konjac glucomannan-ε-polylysine injectable hydrogels for rapid hemostasis and wound healing

Shuo Xu,[a] Jun You,[b] Shaorong Yan,[a] Luting Zhu*[c] and Xiaochen Wu*[a]

Received 21st August 2023,
Accepted 28th September 2023

DOI: 10.1039/d3tb01904g

rsc.li/materials-b

Uncontrollable bleeding is a crucial factor that can lead to fatality. Therefore, the development of hemostatic dressings that enable rapid hemostasis is of utmost importance. Hydrogels with injectability, self-healing ability, and adhesiveness hold significant potential as effective hemostatic dressings. Herein, a composite hydrogel was fabricated by the oxidized Konjac glucomannan and ε-polylysine. After the encapsulation of a hemostatic drug, etamsylate, an oxidized Konjac glucomannan/ε-polylysine/etamsylate (OKGM/PL/E) composite hydrogel that possesses favorable properties including injectability, self-healing ability, tissue adhesiveness, hemocompatibility and cytocompatibility was fabricated. The OKGM/PL/E hydrogel demonstrated the ability to effectively adhere red blood cells and seal wounds, enabling rapid control of hemorrhaging. *In vivo* wound healing experiments confirmed the hemostatic and wound healing efficacy of the OKGM/PL/E hydrogel, highlighting its potential as a valuable hemostatic dressing.

Introduction

Massive bleeding resulting from accidents and trauma can often lead to hemorrhagic shock and pre-hospital deaths, making it a critical health concern worldwide.[1,2] It is crucial to address this issue promptly to prevent hemorrhage-related fatalities, particularly within the first few minutes after an accident. It is therefore essential to maintain immediate and effective hemorrhage control after the accidents to prevent hemorrhage-related deaths.[3,4] To achieve this, traditional dressings with hemostatic ability, such as hemostatic gauze, cotton, and bandages, have been widely used. However, these products have limitations in controlling diffuse and incompressible bleeding, and can even cause secondary damage when removed from wounds.[5] Hence, there is an urgent need to develop advanced hemostatic dressings that fulfill specific criteria. Firstly, they should be cost-effective, ensuring widespread accessibility for users across different backgrounds. Secondly, these dressings should possess biologically active properties, actively promoting blood clotting to effectively cease bleeding. Additionally, they must demonstrate biocompatibility, avoiding any adverse reactions or complications upon contact with the human body. Lastly, strong adhesive properties to tissue are essential for these dressings to maintain their position and effectiveness throughout use.

Injectable, self-healing, and adhesive hydrogels have emerged as the ideal choice for hemostatic dressings due to their distinct properties. Extensive research has shown that these hydrogels can adapt to the shape and size of wounds, repair structural defects within the gel, and adhere to wound tissue even in the presence of exudate and blood.[6–9] By effectively halting bleeding and providing continuous protection to the wound, these hydrogels offer significant advantages in managing hemostasis.[5,10,11] Besides, the three-dimensional network structure of the hydrogels not only provides an optimal environment for tissue regeneration, but also functions as a physical barrier to restrain bacterial infections and create a moist atmosphere to accelerate wound healing.[12] Natural polymer-based injectable hydrogels, in particular, are highly desirable options for hemostatic dressings. These hydrogels offer several advantages, including controllable physical and chemical properties, an excellent biosafety profile, and biodegradability. Among the natural polymers, Konjac glucomannan (KGM), a water-soluble polysaccharide extracted from the tubers of the *Amorphophallus* konjac plant, has shown great promise as a material for wound dressings due to its exceptional biocompatibility, ability to absorb water, capacity to form gels, ease of removal from the wound surface, stimulation of fibroblast proliferation, and capability to accelerate tissue

[a] Department of Pharmacy, College of Chemical Engineering, Qingdao University of Science and Technology, Qingdao 266042, China. E-mail: wxcguest@126.com
[b] Ministry-of-Education Key Laboratory for the Green Preparation and Application of Functional Materials, Hubei University, Youyi Road 368, Wuhan 430062, China
[c] SANKEN (The Institute of Scientific and Industrial Research), Osaka University, 8-1 Mihogaoka, Ibaraki, Osaka 5670047, Japan. E-mail: sharollzhu@eco.sanken.osaka-u.ac.jp

regeneration.[13–16] Moreover, KGM has been proved to be capable to promote the secretion of anti-inflammatory factors, such as IL-10, making it suitable as an immunomodulatory material for wound healing. In addition, hydrogels made from KGM can serve as carriers for various bioactive agents, including polysaccharides, proteins, drugs, growth factors, and nanoparticles. This allows for the incorporation of multiple functionalities, such as mimicking the extracellular matrix, targeted drug delivery, sustained drug release, antibacterial properties, antioxidant properties, and even photothermal therapy.[17,18] For example, silver nanoparticles were incorporated into the composite hydrogels of KGM and chitosan to create a wound dressing with antimicrobial properties;[19] matrine was incorporated into the composite hydrogels of KGM and fish gelatin to inhibit bacterial growth on the wound surface and maintain a suitable physiological environment for wound healing;[20] polydopamine nanoparticles were loaded into composite hydrogels of KGM and xanthan gum for photothermally assisted antibacterial properties and to accelerate wound healing by downregulating the inflammatory response and upregulating vascular reconstruction.[21] However, KGM hydrogels have been rarely utilized in the construction of injectable hydrogels for hemostatic dressings.

Chemical cross-linking is a widely employed method for synthesizing injectable hydrogels. One common strategy involves the condensation of amine groups with aldehyde groups through a Schiff base reaction, resulting in the formation of imine bonds. The Schiff base reaction is easily attainable, reversible, and eliminates the need for external cross-linking agents, making it an appealing choice for the production of biocompatible and injectable hemostatic dressings.[22,23] Aldehyde groups can be introduced into the structure of KGM by oxidizing vicinal hydroxyl groups with sodium periodate. The oxidized KGM (OKGM) can then form composite hydrogels *via* a Schiff base reaction between the aldehyde groups of OKGM and the amino groups of bioactive agents.[24,25] In this study, an injectable and self-healing OKGM/PL hydrogel was fabricated by utilizing the Schiff base reaction between the aldehyde groups of OKGM and the amino-residues of ε-poly-L-lysine (PL). PL is a cationic homopolyamide that possesses remarkable properties such as high water solubility, high thermal stability, biodegradability, and excellent biocompatibility.[26,27] PL possesses cationic properties in neutral aqueous solutions attributed to its amine groups, thereby exhibiting tissue adhesive properties through ionic attraction with the tissue. This characteristic allows for effective adherence between PL and the surrounding tissue.[28] Moreover, PL has been extensively used to enhance cell adhesion,[29] which is beneficial for effective bleeding control of wounds. To further enhance the hemostatic performance of the dressing, a hemostatic drug, etamsylate, was loaded into the OKGM/PL hydrogel (Fig. 1). Etamsylate possesses antihemorrhagic properties that can improve platelet adhesiveness and restore capillary resistance.[30] The physical and chemical properties, biocompatibility, hemostatic performance, and wound healing efficiency of the as-formed OKGM/PL/E composite hydrogels were thoroughly investigated to assess their potential as hemostatic dressings.

Experimental

Materials

Konjac glucomannan and etamsylate were acquired from Shanghai Macklin Biochemical Co., Ltd. ε-Poly-L-lysine·HCl was purchased from Shanghai Aladdin Biochemical Co., Ltd. Sodium tripolyphosphate (STPP) and the dialysis bag (7 kDa cut-off) were purchased from Solarbio Science & Technology Co., Ltd. Other reagents were all from Sinopharm Chemical Reagent Co., Ltd.

Characterization

Morphologies of the samples were analyzed by a JEOL 7401 emission scanning electron microscopy (Japan) at an acceleration voltage of 10 kV. FTIR measurements were performed on a VERTEX 70 Fourier transform infrared spectrometer. UV-vis spectra were obtained using a Molecular Devices SpectraMax i3 (Tacan Austria GmbH, Grodig, Austria). The adhesive strengths of the hydrogels were assessed using an electronic universal testing machine (UTM2502, Shenzhen Suns Technology STOCK Co., Ltd).

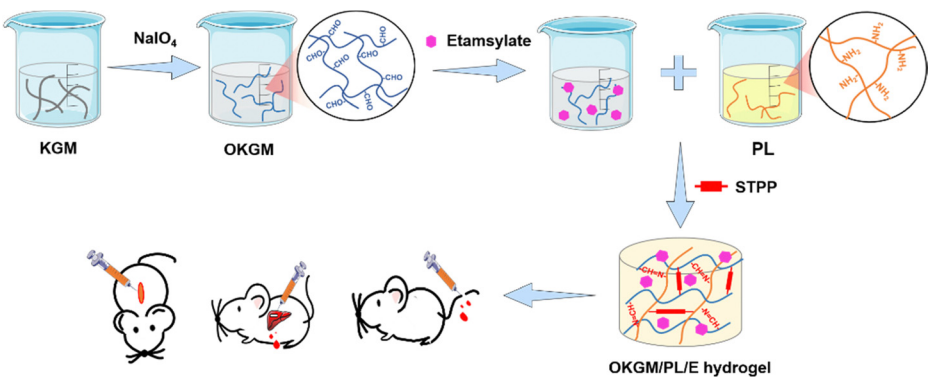

Fig. 1 Schematic illustration of the preparation and application of the OKGM/PL/E hydrogels.

Oxidation of KGM

1.32 g of $NaIO_4$ was added to a 250 mL aqueous solution of 2% (w/v) KGM. The mixture was vigorously stirred at R.T. in a dark environment for 12 h. Then, 10 mL of ethylene glycol was added to consume the excess $NaIO_4$, and the mixture was stirred for an additional 2 h. The reaction mixture was then dialyzed in H_2O using a dialysis bag (7 kDa cut-off) for 3 days. After dialysis, the mixture was centrifuged at 6000 rpm for 10 min to collect the supernatant. Finally, the collected supernatant and freeze-dried to obtain the OKGM.

Preparation of OKGM/PL/E hydrogels

Different amounts of etamsylate (10, 20, and 50 mg) was dissolved in 50 μL of PBS (pH 7.4, 0.01 M), respectively. The solutions were then mixed with 0.5 mL of OKGM solution (0.3 g mL^{-1}, dissolved in PBS). Next, 0.2 mL of PL solution (1 g mL^{-1}, dissolved in PBS) and 0.25 mL of STPP solution (0.28 g mL^{-1}, dissolved in PBS) were added to the mixture. The resulting mixture was stirred evenly to obtain the OKGM/PL/E hydrogels. The OKGM/PL/E hydrogels were denoted OKGM/PL/E*x* where *x* denotes the content of etamsylate (10, 20, or 50 mg mL^{-1} of the hydrogel).

Physicochemical properties of OKGM/PL/E hydrogels

Water content. OKGM/PL/E hydrogels were weighted (m_1), then freeze-dried and weighed again (m_0) to calculate the water content of the hydrogels.

$$\text{Water content}\,(\%) = \frac{m_1 - m_0}{m_1} \times 100\%$$

Blood absorption. The OKGM/PL/E hydrogels were freeze-dried, weighted (m_0), and re-immersed in anticoagulant plasma. The weight of the re-immersed hydrogels was measured (m_t) to calculate the blood absorption ability.

$$\text{Blood absorption}\,(\%) = \frac{m_t - m_0}{m_0} \times 100\%$$

Biocompatibility of OKGM/PL/E hydrogels

Cytotoxicity. Following autoclaving, 1 μL of the OKGM/PL/E hydrogels was dissolved in 20 mL of Dulbecco's Modified Eagle's Medium (DMEM) and diluted 2×10^4 times using DMEM. L929 fibroblasts were seeded onto 96-well plates (4×10^3 cells per well) and incubated for 24 h. Subsequently, 5 μL of the diluted OKGM/PL/E hydrogels was added to each well and incubated for 24–72 h. A blank control without hydrogel was included. Cell viability was evaluated using an MTT assay.

Scratch wound assay. L929s were inoculated onto a 24-well plate (5×10^4 cells per well), a sterile 20–200 μL type pipette tip was used to create a vertical line across the cell monolayer, forming a wound gap. The cells were then washed with PBS, and the DMEM diluted OKGM/PL/E hydrogels were added. With blank DMEM as a control, the scratched wounds were photographed at 0 h, 12 h and 24 h using an Olympus CKX53 fluorescence microscope (Japan).

Irritancy. The chorioallantoic membrane (CAM)-trypan blue staining method was utilized to determine the irritancy of OKGM/PL/E hydrogels. The hydrogels were placed on the surface of a CAM for 5 min, and any changes in the CAM morphology were recorded using a camera. The degree of stimulation was then quantitatively calculated through trypan blue staining. For comparison, a positive control utilizing 0.1 M NaOH and a negative control using normal saline were included.

Hemolysis of OKGM/PL/E hydrogels

A hemolysis assay was conducted to assess the hemocompatibility of OKGM/PL/E hydrogels. To carry out this assay, 0.1 mL of anticoagulant blood, 1 mL of the hydrogels, and 3.5 mL of normal saline were mixed and incubated at 37 °C for 1 hour. Next, the mixture was centrifuged at 3000 rpm for 5 minutes, and the ultraviolet absorption of the supernatant was measured at 545 nm (A_S). A positive control (A_+) was prepared by mixing 0.1 mL of anticoagulant blood with deionized water (3.5 mL), while a negative control (A_-) was prepared by mixing 0.1 mL of anticoagulant blood with normal saline (3.5 mL).

$$\text{Hemolysis} = \frac{A_S - A_-}{A_+ - A_-} \times 100\%$$

Hemostatic ability of OKGM/PL/E hydrogels

Male Kunming mice (aged 5–6 weeks and weighing 30–40 g) and male rats were obtained from Qingdao Darenfucheng Animal Technology Co., Ltd (Qingdao, China). All animal experiments were conducted in compliance with the guidelines of National Research Council's Guide for the Care and Use of Laboratory Animals and was approved of by the Qingdao University of Science and Technology Ethics Committee for Experimentation.

Tail amputation bleeding model[1]. Rats under anesthesia were positioned with their heads elevated higher than their tails. A sterile scalpel was used to cut the tail with a diameter of 4 mm (the tail was placed through the tip of a micropipette to ensure that the circumference of each cut was equal). After 30 seconds of intravenous bleeding, the tail was immersed in an ep-tube containing OKGM/PL/E hydrogels, thereby covering the incision site. The bleeding from the tail was monitored by periodically touching it with a pre-weighed filter paper every 15 seconds until hemostasis was achieved. The filter paper was then re-weighed to determine the amount of blood loss.

Hemorrhaging liver model[31]. Anesthetized rats were positioned on a 45° inclined table, and the abdominal cavity was incised to expose the liver. A pre-weighted filter paper, placed on a parafilm to prevent contamination from abdominal fluid, was positioned beneath the liver. A scalpel was utilized to create a 5 mm long and 3 mm deep incision on the left lobe of the liver. After 15 seconds of bleeding, 1 mL of the OKGM/PL/E hydrogel was injected to cover the incision. Photos were

captured at 30 s, 60 s and 90 s post-injection to visually monitor the hemostasis process. The filter paper, now soaked with blood, was weighed, and the time at which the blood flow visibly ceased was recorded.

Erythrocyte adhesion. To assess erythrocyte adhesion, 2 mL of anticoagulant blood was centrifugated at 1000 rpm for 20 min to abandon the supernatant. Next, 8 mL of normal saline was added and mixed with the sediment to form a suspension of red blood cells. Subsequently, 100 μL of this red blood cell suspension was placed onto the surface of OKGM/PL/E hydrogels and incubated at 37 °C for 30 minutes. Unadhered red blood cells were removed by oblique suction and then ruptured by adding 10 mL of H_2O. The resulting mixture was centrifuged at 2000 rpm for 5 minutes to separate the supernatant. The absorbance of the supernatant at 545 nm was acquired on an HBS-ScanX microplate reader to determine the erythrocyte adhesion rate. The absorbance without (A_0) and with (A_s) the presence of OKGM/PL/E hydrogels were recorded for comparison.

$$\text{Adhered RBCs}\,(\%) = \frac{A_0 - A_s}{A_0} \times 100\%$$

In vivo wound healing efficacy of OKGM/PL/E hydrogels

A full-thickness skin defect model was employed to assess the effectiveness of wound healing. In this model, a 12 mm-long spindle-shaped full-thickness wound was created on the dorsal area of each mouse. The control group underwent no treatment, whereas the remaining groups received various treatments. Specifically, 0.3 mL of etamsylate, OKGM/PL hydrogels, OKGM/PL/E_{20} hydrogels, and OKGM/PL/E_{50} hydrogels were administered and applied to cover the wounds. The wounds were subsequently wrapped in gauze and secured with bandages. Dressings were changed every 2 days throughout the study. Photographs of the wounds were taken every two days using a camera. The wound area was measured and recorded at 3, 5, 7, and 9 days after the treatments, allowing the calculation of wound closure. S_0 and S_N represented the wound area of 0 and N days, respectively (N = 3, 5, 7 and 9).

$$\text{Wound closure}\,(\%) = \frac{S_0 - S_N}{S_0} \times 100\%$$

On the 5th day, the entire wound surface of skin tissue was collected and stained with Masson's trichrome.

Statistical analysis

All experiments were replicated at least 3 times, and statistical analysis was conducted using one-way analysis of variance (ANOVA) to determine the significant differences between data. $p < 0.05$ was considered statistically significant.

Results and discussion

As depicted in Fig. 1 and 2A, aldehyde groups were incorporated into KGM following the protocol described in the literature.[32] This involved the oxidation of vicinal hydroxyl groups with the use of $NaIO_4$. FT-IR spectra were utilized to verify the presence of aldehyde in OKGM (Fig. 2B). The spectrum of OKGM exhibited a new peak at 1735 cm^{-1}, indicating the characteristic vibration of the C═O group in the aldehyde. This confirmed the successful oxidation of KGM. Subsequently, OKGM acted as a supramolecular crosslinker and interacted with PL through the Schiff base reaction to form hydrogels (Fig. 2C). To enhance the stability of the hydrogel system, STPP was incorporated. STPP not only formed phosphate linkages between the intermolecular hydroxyl groups of OKGM,[14] but also crosslinked ionically with the positively charged amine groups of PL *via* its negatively charged polyphosphate ions (Fig. 1).[33,34] The crosslinking reaction occurred under mild conditions, resulting in the formation of a uniform, semi-transparent OKGM/PL hydrogel (Fig. 2D). The SEM image in Fig. 2E depicted the interconnected three-dimensional network structure of the OKGM/PL hydrogel. The presence of porous and irregular networks within the hydrogel may enhance its ability to absorb wound exudates and facilitate nutrient exchange at the wound site.

The OKGM/PL hydrogel displayed excellent adhesiveness and high stretchability, as it could be stretched to more than four times its initial length without cracking (Fig. 2F). Significantly, the OKGM/PL hydrogels demonstrated the ability to be extruded through a syringe needle and injected onto a glass dish to form specific shapes, as shown in Fig. 2F. These injected hydrogels adhered firmly to the surface of the dish, maintaining stable shapes without any displacement. This clearly indicates the injectability of the OKGM/PL hydrogels and highlights their adhesive properties. Consequently, the OKGM/PL hydrogel holds promise for filling irregular wounds and effectively sealing joint wounds. The self-healing properties of the OKGM/PL hydrogels were further investigated. As shown in the photo of Fig. 2G, two hydrogels with distinct colors were placed in contact with each other for a duration of 10 minutes, without any external intervention. Remarkably, it was observed that the two hydrogels seamlessly fused together, with no visible boundary at the contact interface. They merged completely, resulting in the formation of a homogeneous hydrogel, confirmed the self-healing capability of the hydrogels. The OKGM/PL hydrogel exhibited a multitude of favorable properties, including high stretchability, injectability, and self-healing, making it an ideal candidate for hemostatic dressings.

To enhance the functionality of the hydrogel, a hemostatic agent, etamsylate,[35] was incorporated into the matrix of the OKGM/PL hydrogel to form OKGM/PL/E composite hydrogels. As illustrated in Fig. 3A, the FT-IR spectrum of OKGM/PL revealed an important difference compared to the spectrum of OKGM. Specifically, the characteristic peak associated with the C═O vibration of the aldehyde groups at 1735 cm^{-1} disappeared. This disappearance can be attributed to the reaction between OKGM and PL, resulting in the formation of OKGM/PL. After the loading of etamsylate, the OKGM/PL/E hydrogels exhibited characteristic peaks of etamsylate, indicating its successful loading. The UV-vis spectrum presented

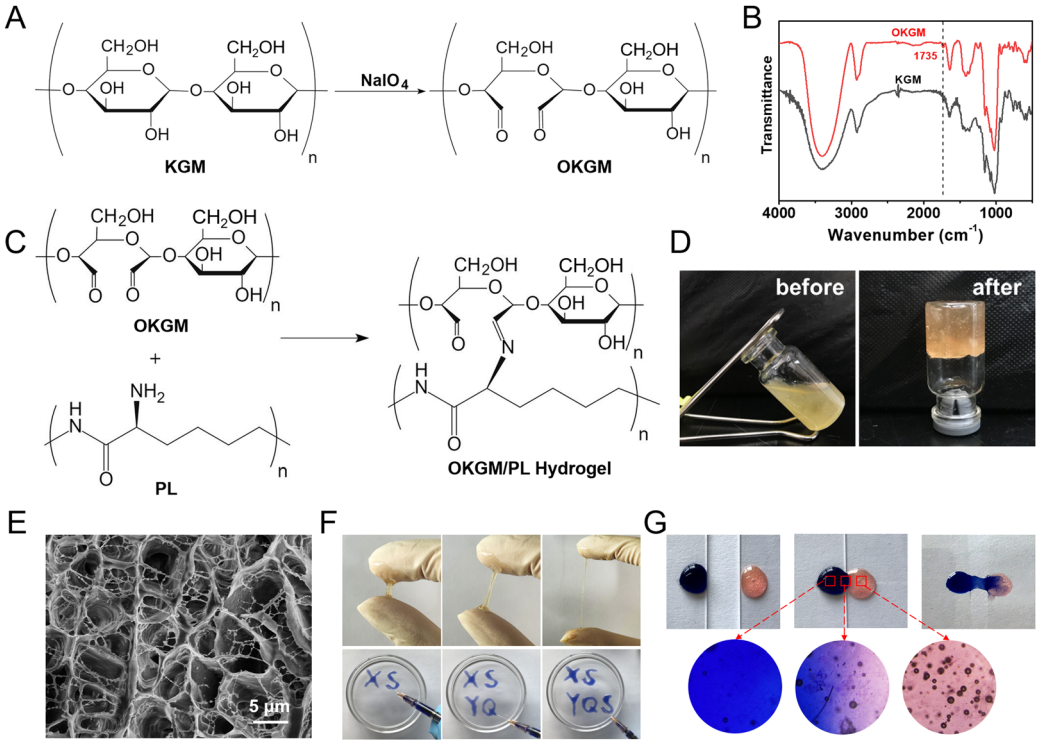

Fig. 2 (A) Oxidation of KGM to OKGM. (B) FT-IR spectra of KGM and OKGM. (C) Chemical crosslinking of OKGM with PL. (D) Photographs of the OKGM/PL hydrogel before (left) and after (right) gelation. (E) SEM image of OKGM/PL hydrogels. (F) Stretchable and injectable test of OKGM/PL hydrogels. (G) Photographs of the restoration of OKGM/PL hydrogels.

similar results: the OKGM/PL/E hydrogels exhibited the characteristic absorption peak of etamsylate at 300 nm (Fig. 3B), confirming the loading of etamsylate.

A desirable hydrogel dressing should have a high-water content to effectively absorb the wound fluid and the exudate, maintain an appropriate moisture level in the wound, facilitate softening of necrotic tissue, and aid in debridement. The OKGM/PL/E hydrogels demonstrated high water content, and the incorporation of etamsylate did not negatively affect the water content (Fig. 3C). For instance, the water content of OKGM/PL, OKGM/PL/E_{10}, OKGM/PL/E_{20} and OKGM/PL/E_{50} hydrogels was 67.2%, 66.0%, 66.6% and 65.6%, respectively. The blood absorption capacity of the OKGM/PL/E hydrogels was depicted in Fig. 3D. The freeze-dried OKGM/PL/E hydrogels possessed a remarkable ability to quickly absorb a substantial amount of blood. Notably, the blood absorption content and the time taken to reach equilibrium remained relatively consistent across different loading amounts of etamsylate in the composite hydrogels. For instance, the OKGM/PL hydrogel exhibited a blood absorption capacity of 811%, while the OKGM/PL/E_{50} hydrogel demonstrated a blood absorption capacity of 818%. The blood absorption capabilities of these hydrogels make them well-suited for use as hemostatic dressings.

To effectively stop bleeding, absorb blood, and prevent potential bacterial colonization, hemostatic hydrogel dressings should possess strong tissue adhesiveness. This enables them to adhere effectively to the wound site. A lap shear test was applied to assess the adhesive properties of the OKGM/PL/E hydrogels (Fig. 3E–G). As depicted schematically and exemplified in the photograph, the OKGM/PL/E hydrogel was sandwiched between two pieces of freshly wetted porcine skin, which mimics the biological properties of the human skin. The adhesive strength of the OKGM/PL/E hydrogels, as demonstrated in Fig. 3G, showed an adhesion strength of 9.1–11.3 kPa with no significant difference between groups. This indicated that the varying amounts of loaded etamsylate had no adverse effect on the adhesive strength values of the hydrogel. The OKGM/PL/E hydrogel demonstrated excellent adhesive behavior to various visceral tissues of mice (Fig. 3H). The organs (*e.g.*, heart, liver, spleen, lungs, and kidneys) can firmly adhere to the OKGM/PL/E hydrogels without any external assistance. Additionally, the hydrogel displayed a strong adherence to stretched, twisted, and squeezed porcine skin, as shown in Fig. 3I. These consistent results highlighted the remarkable adhesion ability of the OKGM/PL/E hydrogels under wet and dynamic conditions,[36] indicating their potential for tightly adhering to tissues and delivering hemostatic effects.

In order to be used as wound dressings, the hydrogel must exhibit excellent biocompatibility. The cytotoxicity of the hydrogels was evaluated by an MTT assay against L929 cells (Fig. 4A and B). During 3 days of incubation, the viability of cells treated with OKGM/PL hydrogels was comparable to the control group, indicating the good biocompatibility of the OKGM/PL hydrogels. The presence of etamsylate did not negatively affect the cytocompatibility of the OKGM/PL hydrogels. For example, after 3 days of incubation, the viability of L929s treated with

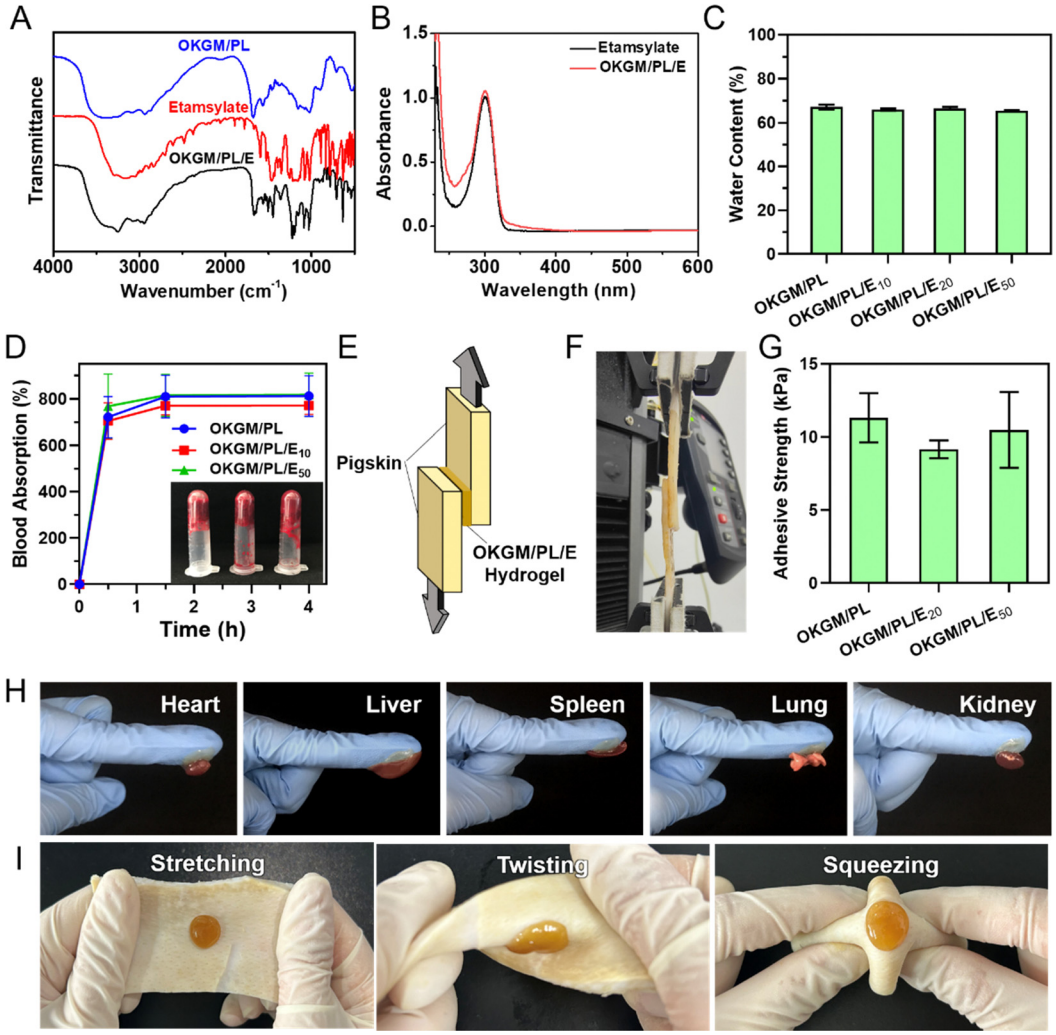

Fig. 3 (A) FTIR spectra, (B) UV spectra, (C) water content, and (D) blood absorption of the OKGM/PL/E hydrogels. (E) Schematic illustration and (F) photograph of the lap shear experiment. (G) Adhesive strength of the OKGM/PL/E hydrogels. (H) and (I) Photographs showing the adhesion property of the OKGM/PL/E_{50} hydrogels.

OKGM/PL/E_{20} hydrogels was 123.8%, and the viability of L929s treated with OKGM/PL/E_{50} hydrogels was 128.6%, exhibiting the satisfactory cytocompatibility of the OKGM/PL/E hydrogels.

Furthermore, a scratch assay was conducted to evaluate the effect of the OKGM/PL/E hydrogels on the migration of L929s (Fig. 4C and D). Both the OKGM/PL and OKGM/PL/E hydrogels exhibited a tendency to promote cell migration. For example, the OKGM/PL/E_{50} hydrogel significantly enhanced the migration of L929s within 24 hours, with approximately 60.4% of the wound area healed due to cell migration, compared with 29.1% of the control group. The effect of OKGM/PL/E hydrogels was statistically different from that of the control group, highlighting the great potential of the OKGM/PL/E hydrogels in promoting wound healing. KGM stands out as an excellent matrix material due to its favorable biocompatibility and biodegradability.[37] Similarly, PL also possesses remarkable biocompatibility and has been extensively employed to enhance cell adhesion.[29,38] Consequently, the incorporation of PL in the OKGM/PL/E hydrogel further enhances its cell affinity. This synergistic effect likely contributes to the hydrogel's ability to promote L929 cells migration.

When used as dressings, it is crucial for the OKGM/PL/E hydrogels to not cause irritation to biological membranes. In the case of direct contact with CAM for 5 minutes, the hydrogels showed no signs of injuring or causing hemorrhage to the veins, arteries, or capillaries of the CAM, as depicted in Fig. 5A. To assess the level of CAM irritation, the absorption of trypan blue at the hydrogel treatment site was measured. Fig. 5B clearly indicated that the OKGM/PL/E hydrogels caused minimal irritation to the CAM, with significantly different results from the positive control, confirming the excellent biocompatibility of the hydrogels. Furthermore, for effective hemostatic dressings, it is important for them to have a minimal impact on hemolysis when in contact with bleeding wounds. After incubation with blood samples for an hour, no observable toxicity against erythrocytes was noticed, as shown in Fig. 5C. None of the OKGM/PL/E hydrogels, regardless of drug loading amount, resulted in any hemolysis. The hemolysis rate of the hydrogels

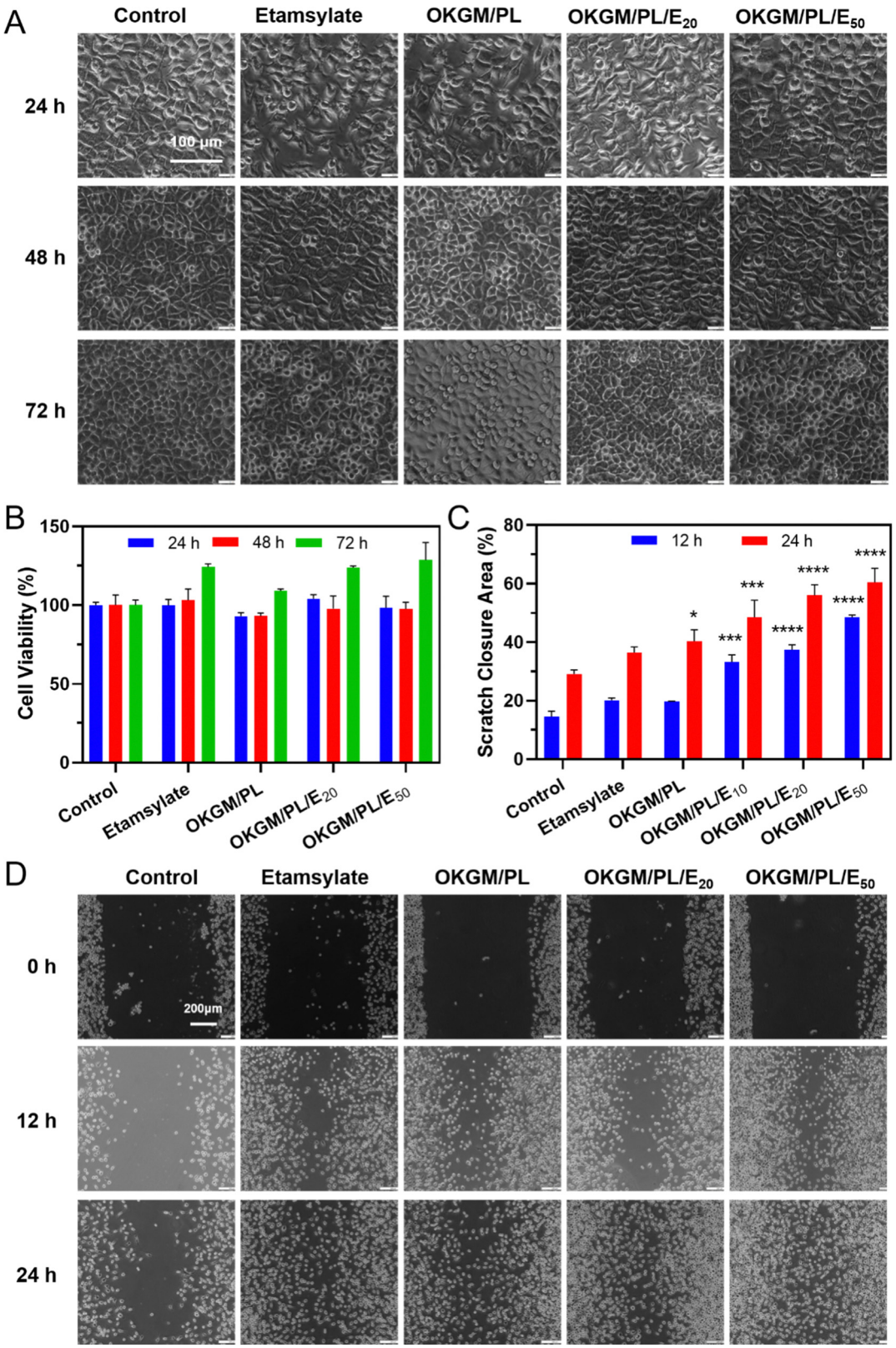

Fig. 4 (A) Micrographs and (B) cell viability of L929s after 24, 48 and 72 h of different treatments. (C) Scratch closure area calculated from (D), *$p < 0.05$, ***$p < 0.001$, and ****$p < 0.0001$ compared to the control group on the same day. (D) Micrographs of scratch wounds at 0, 12 and 24 h after different treatments.

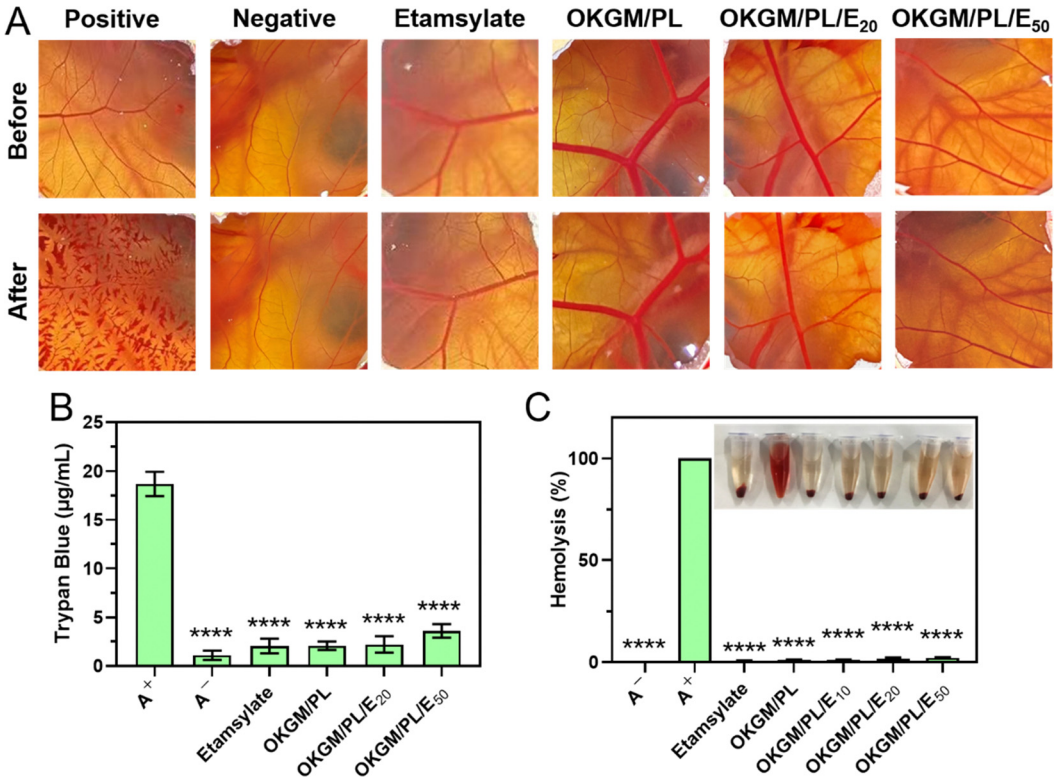

Fig. 5 (A) Photographs of CAM after different treatments. (B) Trypan blue staining results of CAM. (C) Hemolysis of the OKGM/PL/E hydrogels. ****$p <$ 0.0001 compared to the positive control group.

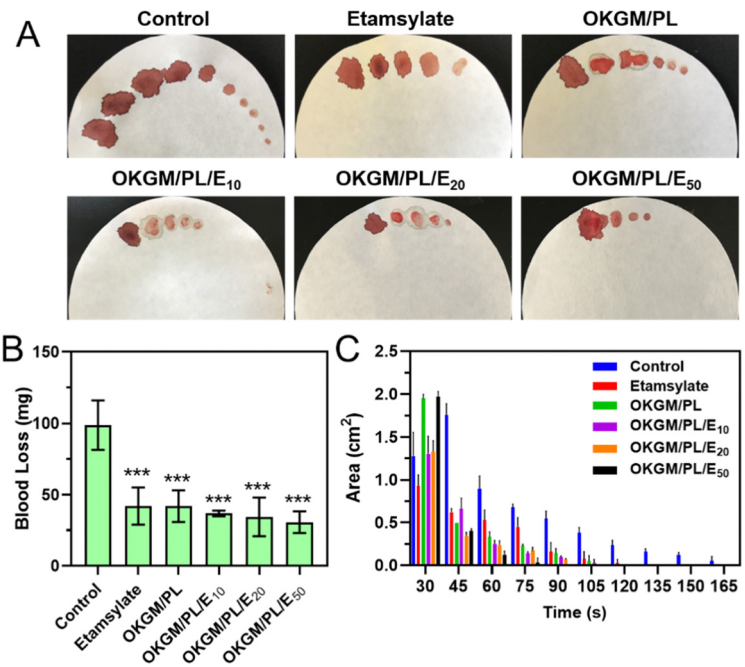

Fig. 6 Effect of the OKGM/PL/E hydrogels on tail amputation. (A) Photographs of blood loss every 15 s until the hemostasis. (B) Total blood loss after 165 s treatment, ***$p <$ 0.001 compared to the control group. (C) Blood area on filter papers *versus* time calculated from (A).

was below 3%, indicating exceptional hemocompatibility and suggesting their safety as hemostatic materials.

The potential application of OKGM/PL/E hydrogels as hemostatic dressings is promising due to their injectability, adhesiveness, and biocompatibility. To evaluate their hemostatic potential, tail amputation was performed as a typical bleeding model (Fig. 6). The hydrogels were immediately applied to the cut tail to assess the hemostatic efficacies. The untreated tail generated a large area of bloodstain on the filter paper, with a total blood loss of 98.7 mg after 165 seconds. Both the individual etamsylate and the OKGM/PL hydrogel can efficiently reduce the blood loss to some extent, which was significantly different from the non-treated control group. After applying the OKGM/PL/E_{20} and OKGM/PL/E_{50} hydrogel, the total blood loss was dramatically reduced, for example, only 30.7 mg of blood was collected after treatment of OKGM/PL/E_{50}, which was ~3 times lower than the control group (Fig. 6B). Moreover, there was almost no subsequent bleeding from the wound to the filter paper after 75 s treatment of the OKGM/PL/E_{50}, as well as 90 s treatment of the OKGM/PL/E_{20} (Fig. 6A and C). That is, the bleeding was rapidly controlled within 75 s of treatment with the OKGM/PL/E_{50} dressing, which was ~2.2 times faster than the control group, suggesting that the hydrogels can act as a barrier to seal the wound and stop bleeding rapidly and constantly.

Similar hemostatic results were observed in the liver incision model of rats (Fig. 7A–D). The application of OKGM/PL/E hydrogels quickly inhibited liver bleeding. For example, the average value of the total blood loss, bleeding distance, and hemostasis time of the OKGM/PL/E_{50} treated group was 49.2 mg, 4.0 cm and 155.3 s, respectively, significantly lower than the non-treated control group, which was 207.9 mg, 10.2 cm and 247.7 s, respectively. Furthermore, the OKGM/PL/E hydrogels demonstrated excellent adhesiveness to bleeding tissues, remaining at the bleeding site without being swept away for more than 5 minutes. This highlighted their ability to effectively adhere to

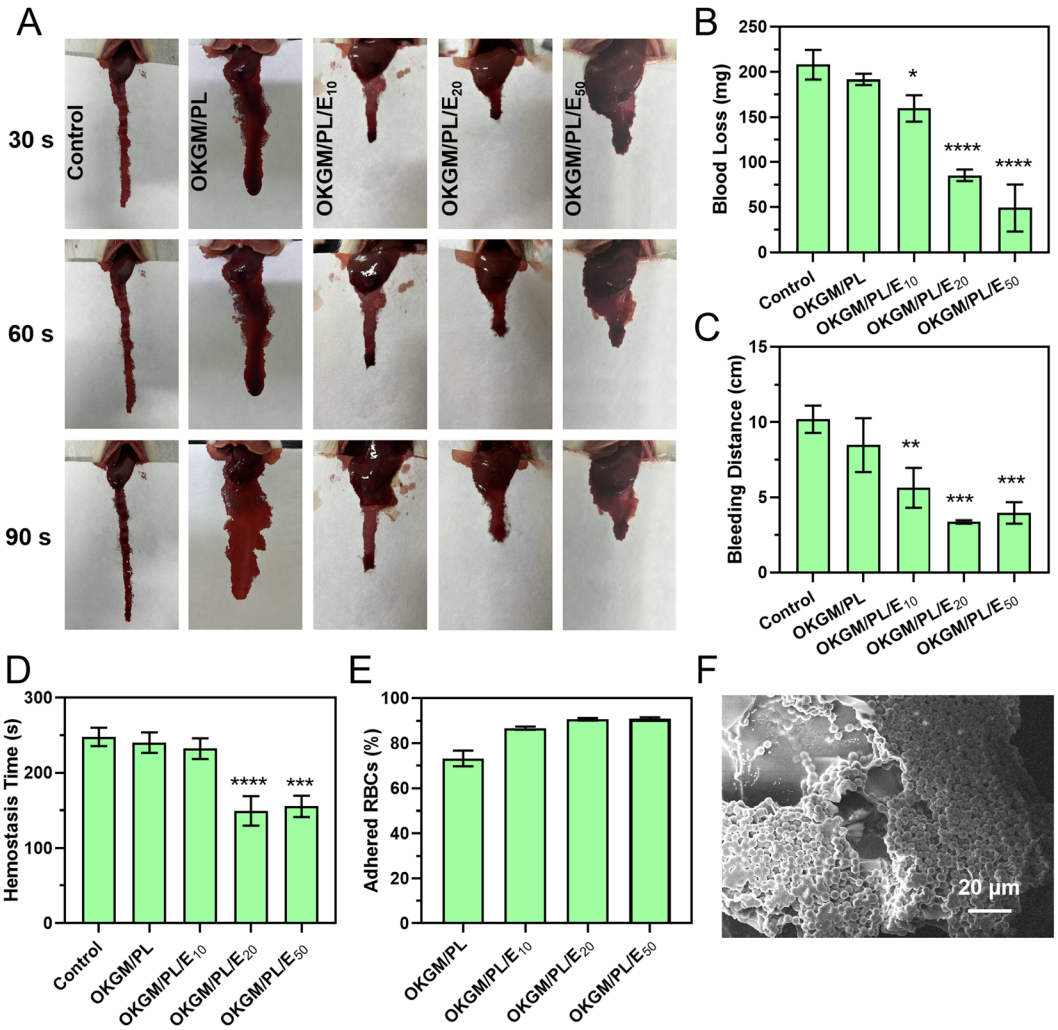

Fig. 7 (A)–(D) Effects of the OKGM/PL/E hydrogels on liver incision. (A) Blood loss of the damaged liver after different treatments for 30 s, 60 s, and 90 s. (B) Blood loss, (C) bleeding distance, and (D) hemostasis time calculated from (A), ****$p < 0.0001$, ***$p < 0.001$, **$p < 0.005$, *$p < 0.05$ compared to the control group. (E) Adhesion of red blood cells (RBCs) by the OKGM/PL/E hydrogels. (F) SEM image of the adhered red blood cells on the surface of an OKGM/PL/E_{50} hydrogel.

the bleeding tissues. The OKGM/PL/E_{50} hydrogel combined the hemostatic ability of etamsylate with the tissue adhesiveness of the OKGM/PL hydrogel. As a result, it exhibited positive hemostatic properties, quickly and thoroughly inhibiting blood loss.

The hemostatic properties of the OKGM/PL/E hydrogels may be partially attributed to their ability to promote surface adhesion of red blood cells. The OKGM/PL/E hydrogels exhibited a strong affinity for red blood cells. Approximately 73.2% of the red blood cells were adhered to the OKGM/PL hydrogel, while 90.9% of the red blood cells were adhered to the OKGM/PL_{50} hydrogel after incubation for 30 min (Fig. 7E). As depicted in Fig. 7F, the OKGM/PL/E_{50} hydrogels displayed significant adherence of red blood cells to their surfaces. The interconnected porous structure and blood absorption ability of the OKGM/PL/E_{50} hydrogel enabled it to rapidly absorb plasma and efficiently concentrate blood, thereby trapping aggregated hemocytes.[39] By promoting the adhesion of red blood cells, the OKGM/PL/E hydrogels enhanced coagulation and facilitated a rapid hemostatic effect.

The *in vivo* hemostatic performance as well as the wound healing efficiency of the OKGM/PL/E hydrogels was further assessed on a full-thickness skin defect model (Fig. 8). The wound closure was monitored every two days from the day of wound creation. Generally, in comparison with the non-treated control group and that treated by etamsylate or OKGM/PL, the wounds managed by the OKGM/PL/E hydrogels exhibited better healing effects. For instance, quantitative statistical analysis showed that on day 5, the wound closure was 87.2% for the OKGM/PL/E_{50} hydrogel treated group, while the value was 40.4%, 51.8%, 59.3%, and 82.5% for the blank control, the etamsylate treated group, the OKGM/PL hydrogel treated group, and the OKGM/PL/E_{20} hydrogel treated group, respectively, demonstrating the high efficiency of the OKGM/PL/E_{50} hydrogel in promoting wound healing (Fig. 8A and B). The OKGM/PL/E hydrogel can firmly adhere to the tissue, absorb wound exudates, prevent wound dehydration while inhibit bleeding to facilitate healing. Masson's trichrome staining of the wound site showed that after the treatment of the OKGM/PL/E_{50} hydrogel, the healed skin was comparable with the normal skin, confirming the overall healing efficacy of the OKGM/PL/E hydrogels (Fig. 8C).

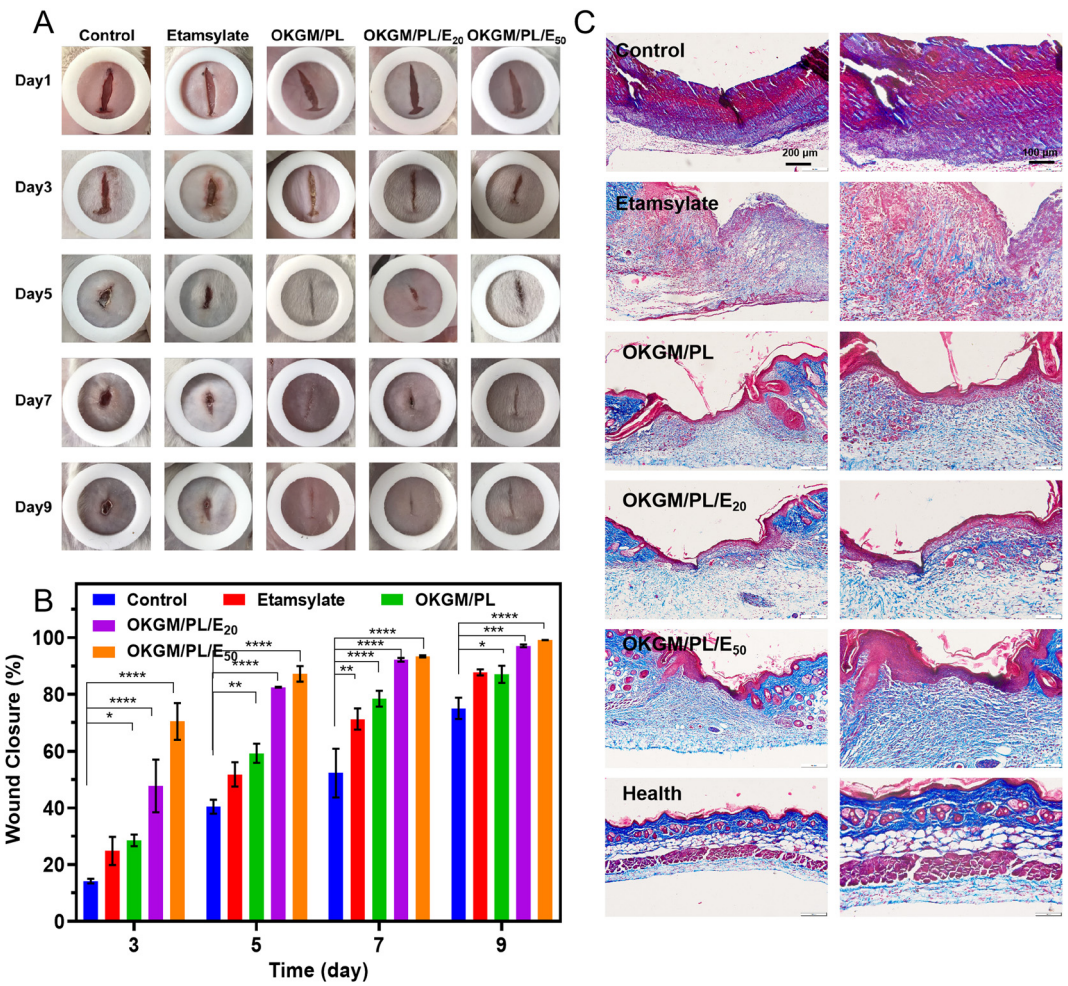

Fig. 8 *In vivo* wound healing and histologic analysis results. (A) Photographs of wounds after different treatments in 9 days. (B) Wound closure calculated from (A), ****$p < 0.0001$, ***$p < 0.001$, **$p < 0.005$, *$p < 0.05$ compared to the control group. (C) Images of Masson's trichrome stained wound tissue after 5 days of different treatments.

Conclusions

In summary, an OKGM/PL/E hydrogel was fabricated with favorable properties. This hydrogel was crosslinked through a *Schiff* base reaction between the aldehyde group of OKGM and the amino group of PL, followed by the loading of a hemostatic drug etamsylate. The OKGM/PL/E hydrogel possessed several remarkable properties, including injectability, self-healing ability, tissue adhesiveness, blood adsorption ability, and biocompatibility, thus could effectively seal different shapes of wounds and realize excellent *in vivo* hemostatic performance. Moreover, the OKGM/PL/E hydrogel could efficiently accelerate wound healing, making it an ideal material for the development of hydrogel dressings with rapid hemostatic properties.

Conflicts of interest

The authors declare no competing financial interest.

Acknowledgements

This work was supported by the Talent Foundation funded by Province and Ministry Co-construction Collaborative Innovation Center of Eco-chemical Engineering (STHGYX2206).

References

1 A. Kumar, D. K. Sah, K. Khanna, Y. Rai, A. K. Yadav, M. S. Ansari and A. N. Bhatt, *Carbohydr. Polym.*, 2023, **299**, 120186.
2 C. Cao, N. Yang, Y. Zhao, D. Yang, Y. Hu, D. Yang, X. Song, W. Wang and X. Dong, *Nano Today*, 2021, **39**, 101165.
3 S. Indrakumar, S. Ghosh, T. K. Dash, V. Mishra, B. Tandon and K. Chatterjee, *Carbohydr. Polym.*, 2023, **304**, 120479.
4 Y. Shi, W. Yu, X. Liang, J. Cheng, Y. Cao, M. Liu, Y. Fang, Z. Yang, H. Liu, H. Wei and G. Zhao, *Carbohydr. Polym.*, 2023, **307**, 120590.
5 Z. Chen, J. Zhao, H. Wu, H. Wang, X. Lu, M.-A. Shahbazi and S. Wang, *Carbohydr. Polym.*, 2023, **303**, 120434.
6 J. He, Z. Zhang, Y. Yang, F. Ren, J. Li, S. Zhu, F. Ma, R. Wu, Y. Lv, G. He, B. Guo and D. Chu, *Nano-Micro Lett.*, 2021, **13**, 80.
7 Y. Liang, H. Xu, Z. Li, A. Zhangji and B. Guo, *Nano-Micro Lett.*, 2022, **14**, 185.
8 B. Guo, R. Dong, Y. Liang and M. Li, *Nat. Rev. Chem.*, 2021, **5**, 773–791.
9 Y. Liang, M. Li, Y. Yang, L. Qiao, H. Xu and B. Guo, *ACS Nano*, 2022, **16**, 3194–3207.
10 Y. Lv, F. Cai, Y. He, L. Li, Y. Huang, J. Yang, Y. Zheng and X. Shi, *Acta Biomater.*, 2023, **159**, 95–110.
11 Y. Wang, M. Yang and Z. Zhao, *Carbohydr. Polym.*, 2023, **310**, 120723.
12 H. Cao, D. Xiang, X. Zhou, P. Yue, Y. Zou, Z. Zhong, Y. Ma, L. Wang, S. Wu and Q. Ye, *Carbohydr. Polym.*, 2023, **307**, 120609.
13 H. Chen, J. Cheng, L. Ran, K. Yu, B. Lu, G. Lan, F. Dai and F. Lu, *Carbohydr. Polym.*, 2018, **201**, 522–531.
14 P. K. Veerasubramanian, P. Thangavel, R. Kannan, S. Chakraborty, B. Ramachandran, L. Suguna and V. Muthuvijayan, *Colloids Surf., B*, 2018, **165**, 92–102.
15 Y. Xie, Z.-x Yi, J.-x Wang, T.-g Hou and Q. Jiang, *Int. J. Biol. Macromol.*, 2018, **112**, 1225–1233.
16 L. Zhu, J. Chen, X. Mao and S. Tang, *Mater. Sci. Eng., C*, 2021, **129**, 112374.
17 N. Zhou, S. Zheng, W. Xie, G. Cao, L. Wang and J. Pang, *J. Appl. Polym. Sci.*, 2022, **139**, 51780.
18 R. D. Devaraj, C. K. Reddy and B. Xu, *Int. J. Biol. Macromol.*, 2019, **126**, 273–281.
19 Y. Jiang, J. Huang, X. Wu, Y. Ren, Z. Li and J. Ren, *Int. J. Biol. Macromol.*, 2020, **149**, 148–157.
20 L. Zhou, T. Xu, J. Yan, X. Li, Y. Xie and H. Chen, *Food Hydrocolloids*, 2020, **104**, 105702.
21 Q. Zeng, Y. Qian, Y. Huang, F. Ding, X. Qi and J. Shen, *Bioact. Mater.*, 2021, **6**, 2647–2657.
22 C. Mo, L. Xiang and Y. Chen, *Macromol. Rapid Commun.*, 2021, **42**, 2100025.
23 J. Yang and S. Wang, *Gels*, 2023, **9**, 138.
24 D. Yang, Y. Yuan, L. Wang, X. Wang, R. Mu, J. Pang, J. Xiao and Y. Zheng, *Int. J. Mol. Sci.*, 2017, **18**, 2250.
25 F. Zhu, *Food Chem.*, 2018, **256**, 419–426.
26 Y. Wang, H. Cao and X. Wang, *Mater. Chem. Phys.*, 2020, **248**, 122902.
27 H. Liu, Z. Li, Y. Zhao, Y. Feng, A. V. Zvyagin, J. Wang, X. Yang, B. Yang and Q. Lin, *ACS Appl. Mater. Interfaces*, 2021, **13**, 26770–26781.
28 W. Nie, X. Yuan, J. Zhao, Y. Zhou and H. Bao, *Carbohydr. Polym.*, 2013, **96**, 342–348.
29 Y. Sun, X. Chi, H. Meng, M. Ma, J. Wang, Z. Feng, Q. Quan, G. Liu, Y. Wang, Y. Xie, Y. Zheng and J. Peng, *Bioact. Mater.*, 2021, **6**, 3987–3998.
30 P. Suchý, A. Paprskářová, M. Chalupová, L. Marholdová, K. Nešporová, J. Klusáková, G. Kuzmínová, M. Hendrych and V. Velebný, *Materials*, 2020, **13**, 1627.
31 W. Feng and Z. Wang, *Carbohydr. Polym.*, 2022, **294**, 119824.
32 J. Luan, K. Wu, C. Li, J. Liu, X. Ni, M. Xiao, Y. Xu, Y. Kuang and F. Jiang, *Carbohydr. Polym.*, 2017, **171**, 9–17.
33 C. Wu, Y. Li, Y. Du, L. Wang, C. Tong, Y. Hu, J. Pang and Z. Yan, *Food Hydrocolloids*, 2019, **89**, 682–690.
34 G. Patil, A. Torris, P. R. Suresha, S. Jadhav, M. V. Badiger and V. Ghormade, *Colloids Surf., B*, 2021, **198**, 111454.
35 M. Y. Cobo-Nuñez, M. El Assar, P. Cuevas, A. Sánchez-Ferrer, J. Martínez-González, L. Rodríguez-Mañas and J. Angulo, *Eur. J. Pharmacol.*, 2018, **827**, 167–172.
36 W. Xue, R. Yang, S. Liu, Y. Pu, P. Wang, W. Zhang, X. Tan and B. Chi, *Biomater. Sci.*, 2022, **10**, 2417–2427.
37 H. R. Nie, X. X. Shen, Z. H. Zhou, Q. S. Jiang, Y. W. Chen, A. Xie, Y. Wang and C. C. Han, *Carbohydr. Polym.*, 2011, **85**, 681–686.
38 S. Some, S.-M. Ho, P. Dua, E. Hwang, Y. H. Shin, H. Yoo, J.-S. Kang, D.-K. Lee and H. Lee, *ACS Nano*, 2012, **6**, 7151–7161.
39 R. Cui, F. Chen, Y. Zhao, W. Huang and C. Liu, *J. Mater. Chem. B*, 2020, **8**, 8282–8293.

